



Research Article

Ginsenoside F1 attenuates pirarubicin-induced cardiotoxicity by modulating Nrf2 and AKT/Bcl-2 signaling pathways

Yang Zhang ^{a, b, 1}, Jiulong Ma ^{a, 1}, Shan Liu ^a, Chen Chen ^a, Qi Li ^a, Meng Qin ^a, Liqun Ren ^{a, *}^a Department of Experimental Pharmacology and Toxicology, School of Pharmacy, Jilin University, Jilin, China^b Department of Rehabilitation Medicine, Nanjing University of Chinese Medicine, Nanjing, China

ARTICLE INFO

Article history:

Received 8 February 2022

Received in revised form

22 June 2022

Accepted 28 June 2022

Available online 5 July 2022

Keywords:

Ginsenoside F1

Pirarubicin

Cardiotoxicity

Oxidative stress

Apoptosis

ABSTRACT

Background: Pirarubicin (THP) is an anthracycline antibiotic used to treat various malignancies in humans. The clinical usefulness of THP is unfortunately limited by its dose-related cardiotoxicity. Ginsenoside F1 (GF1) is a metabolite formed when the ginsenosides Re and Rg1 are hydrolyzed. However, the protective effects and underlying mechanisms of GF1 on THP-induced cardiotoxicity remain unclear. **Methods:** We investigated the anti-apoptotic and anti-oxidative stress effects of GF1 on an *in vitro* model, using H9c2 cells stimulated by THP, plus trigonelline or AKT inhibitor imidazoquinoxaline (IMQ), as well as an *in vivo* model using THP-induced cardiotoxicity in rats. Using an enzyme-linked immunosorbent test, the levels of malondialdehyde (MDA), brain natriuretic peptide (BNP), creatine kinase (CK-MB), cardiac troponin (c-TnT), lactate dehydrogenase (LDH), superoxide dismutase (SOD) and glutathione (GSH) were determined. Nuclear factor (erythroid-derived2)-like 2 (Nrf2) and the expression of Nrf2 target genes, including heme oxygenase-1 (HO-1), glutathione-S-transferase (Gst), glutamate-cysteine ligase modifier subunit (GCLM), and expression levels of AKT/Bcl-2 signaling pathway proteins were detected using Western blot analysis.

Results: THP-induced myocardial histopathological damage, electrocardiogram (ECG) abnormalities, and cardiac dysfunction were reduced *in vivo* by GF1. GF1 also decreased MDA, BNP, CK-MB, c-TnT, and LDH levels in the serum, while raising SOD and GSH levels. GF1 boosted Nrf2 nuclear translocation and Nrf2 target gene expression, including HO-1, Gst, and GCLM. Furthermore, GF1 regulated apoptosis by activating AKT/Bcl-2 signaling pathways. Employing Nrf2 inhibitor trigonelline and AKT inhibitor IMQ revealed that GF1 lacked antioxidant and anti-apoptotic effects.

Conclusion: In conclusion, GF1 was found to alleviate THP-induced cardiotoxicity via modulating Nrf2 and AKT/Bcl-2 signaling pathways, ultimately alleviating myocardial oxidative stress and apoptosis.

© 2022 The Korean Society of Ginseng. Publishing services by Elsevier B.V. This is an open access article under the CC BY-NC-ND license (<http://creativecommons.org/licenses/by-nc-nd/4.0/>).

1. Introduction

Because of its high efficiency and broad-spectrum, pirarubicin (THP), an anthracycline antibiotic, is commonly utilized in clinical practice to treat malignancies. [1]. However, it has been determined to cause toxicity [2], limiting its medical use [3]. The most serious toxicity of THP is cardiotoxicity, which worsens with increasing medication doses [4].

Ginsenoside F1 (GF1) is a metabolite formed when the ginsenosides Re and Rg1 are hydrolyzed [5]. Recent research suggests that GF1 has potent anti-aging, anti-oxidation, and anti-cancer properties [6]. Furthermore, it's great that we were able to extract a large amount of GF1 through ginsenoside Rg1 bioconversion, which encourages GF1 research [5,7].

Nrf2 is a transcription factor activated by oxidative stress that increases antioxidant and detoxifying enzymes to combat ROS and toxic metabolites [8]. In normal conditions, Nrf2 is anchored in the cytoplasm [9]. When Nrf2 translocates into the nucleus in response to oxidative stress, it regulates the expression stages of several anti-oxidative genes and enzymes [10,11]. Apoptosis plays an important role in the pathogenesis of THP-induced cardiotoxicity via activating caspases [12]. Many proteins, such as caspases, promote apoptosis, whereas Bcl-2 family proteins, such as Bcl-2, suppress

* Corresponding author. Department of Experimental Pharmacology and Toxicology, School of Pharmacy, Jilin University, 1266 Fujin Road, Changchun, Jilin, 130021, China.

E-mail addresses: renlq@jlu.edu.cn, renlq630210@163.com (L. Ren).

¹ Co-First author.

apoptosis [13]. When Bcl-2 expression is reduced, cytochrome c (cyt-c) is released through the mitochondrial membrane, resulting in apoptosome formation [14,15]. The apoptosome turns to activate the effector caspase 3. In addition, protein kinase B (AKT) is a critical molecule in THP-induced apoptosis. AKT phosphorylation can activate Bcl-2 and protect cardiomyocytes from apoptosis [16].

Therefore, this work aimed to investigate the defensive impact of GF1 against THP-induced cardiotoxicity and determine whether or not this effect was mediated by adjusting Nrf2 and AKT/Bcl-2 signaling pathways, ultimately regulating myocardial oxidative stress and apoptosis.

2. Materials and methods

2.1. Chemicals and reagents

Ginsenoside F1 (GF1, purity >98.0%) was obtained from Chengdu GELIPU Biotechnology Co., Ltd (Chengdu, China). HAN HUI PHARMACEUTICALS Co., Ltd. (Jiangsu, China) provided the pirarubicin (THP). Jiangsu Aosaikang Pharmaceutical Co., Ltd. (Jiangsu, China) provided the dexrazoxane (DZR). Shanghai Meixuan Biological Science and Technology Ltd (Shanghai, China) provided test kits for BNP, CK-MB, and c-TnT. Commercial assay kits for hematoxylin-eosin (HE) dye, MDA, LDH, SOD, and GSH kits were obtained from Nanjing Jian Cheng Biological Engineering Research Institute (Nanjing, China). Anti-AKT, anti-p-AKT, anti-Bcl-2, anti-caspase 3, anti-pro-caspase 9, anti-GAPDH, anti-Bax, anti-Nrf2, anti-Lamin B, anti-Keap1, anti-HO-1, anti-Gst, and anti-GCLM antibodies were purchased from Abcam (MA, USA). Imidazoquinoxaline (AKT inhibitor, IMQ) and nuclear and cytoplasmic Protein Extraction Kit were obtained from Beyotime Institute of Biotechnology (Jiangsu, China). Trigonelline (Nrf2 inhibitor) was supplied by MedChemExpress (Shanghai, China). Methyl thiazolyl tetrazolium (MTT, A100793) was purchased from Sangon Biotech (Shanghai) Co., Ltd. All other reagents and chemicals, unless indicated, were obtained from Beijing Chemical Works (Beijing, China).

2.2. Animals and experimental protocol

This study was approved by the Animal Care and Ethics Committee of Jilin University (Changchun, China; Grant no. 20170503) and was performed following the National Institutes of Health Guidelines for the Care and Use of Laboratory Animals. The Animal Experiment Center of Jilin University provided 40 male Wistar rats of clean grade, weighing 200 ± 20 g. The rats were housed in a typical environment with a temperature of $22 \pm 3^\circ\text{C}$, a humidity of $50 \pm 10\%$, and 12 h of light/dark cycles. All experimental animals were euthanized by inhalation of CO_2 (30% volume displacement per minute).

After adaptive breeding for one week, the rats were randomly divided into five groups ($n=8$): (1) Control (CON), (2) THP (3 mg/kg/weekly), (3) THP + Dexrazoxane (DZR) (30 mg/kg/weekly), (4) THP + low-dose GF1L (25 mg/kg/d), and (5) THP + high-dose GF1H (50 mg/kg/d). GF1-treated rats were given varying doses of GF1 every day for a week before receiving THP injections. For a week, THP and DZR-treated rats were given sodium carboxymethylcellulose (CMC-Na) via gavage. In addition, a weekly dose of 3 mg/kg THP was administered for six weeks through caudal vein injection to develop the cardiotoxicity model [20]. DZR (30 mg/kg) was subsequently given to rats through intraperitoneal injection once a week for six weeks. In the control group, rats were given CMC-Na via gavage for seven days, then saline via caudal vein injection for six weeks.

2.3. Detection of hemodynamic indexes and electrocardiogram

Pentobarbital sodium intraperitoneal injection was used to anesthetize the rats. A plastic cannula with an inner diameter of 1 mm was placed into the left ventricle of rats and attached to the BL-420E biological function experiment system after the right common carotid artery was fixed and separated [4]. We measured the left ventricular systolic pressure (LVSP), left ventricular end-diastolic pressure (LVEDP), and the maximal rate of change in left ventricular pressure ($\pm dp/dt_{\text{max}}$). The rat ECG was examined using the conventional limb II.

2.4. Assessment of biochemical parameters

Blood samples were taken from the abdominal aorta and centrifuged at 3000 rpm for 15 min after being left to stand for six hours. Following that, serum levels of BNP, CK-MB, c-TnT, MDA, LDH, GSH, and SOD were measured using ELISA detection kits, as directed by the manufacturer.

2.5. Hematoxylin-eosin (HE) staining

The cardiac samples were fixed with 10% formalin before paraffin embedding. Each group's paraffin slices were stained with HE solution. At $200\times$ magnification, HE-stained pictures were viewed using a Nikon Eclipse 80i microscope (Nikon, Chiyoda, Japan).

2.6. Immunohistochemistry (IHC) and immunofluorescence (IF) analysis

During IHC staining, paraffin slices were deparaffinized, hydrated, and then incubated at 4°C in a humidified chamber overnight [17], with primary antibodies against cytochrome c (cyt-c) (1:50) and phospho-AKT (p-AKT) (1:100). They were then incubated with horseradish peroxidase-conjugated secondary antibodies at 25°C for 20 min and stained with hematoxylin for 8 min.

During immunofluorescence staining, cardiac sections were deparaffinized, hydrated, and then incubated at 4°C in a humidified chamber overnight, with primary antibody against caspase 3, followed by incubation with secondary antibodies at 25°C for 20 min [17]. The nucleus was stained with DAPI.

IHC and IF stained images were visualized using a Nikon Eclipse 80i microscope (Nikon, Chiyoda, Japan) at $200\times$ magnification, and the intensity of positive cell expression was quantified with Image-Pro Plus 6.0.

2.7. Separation of nucleus and cytoplasm

Under low osmotic pressure conditions, the cells were fully swelled, the cell membrane was destroyed, cytoplasmic proteins were released, and then the nucleus pellet was obtained by centrifugation [18]. Finally, a high-salt nucleoprotein extraction reagent was used to extract the nucleoproteins.

2.8. Cell culture

Rat cardiac myocytes (H9c2) were obtained from the American Type Culture Collection. H9c2 cells were grown in DMEM (containing 4.5 mg/mL of glucose), supplemented with 10% foetal bovine serum. Cells were cultured in $5\% \text{CO}_2$ at 37°C , and the culture medium was replaced every 2 to 3 days.

2.9. Cytotoxicity of GF1 and THP-induced cell injury/GF1 inhibits THP-induced cell injury

The cells were seeded into 96-well plates at a density of 5×10^4 cells/mL earlier than therapy, with distinct concentrations of GF1 (0, 10, 20, 40, 60, and 80 μM) or THP (1, 3, 5, 7, and 9 μM). The cells in CON were handled with equal quantities of serum-free medium. Furthermore, cell viability was determined using the MTT test after 6, 12, 24, and 36 h incubation.

H9c2 cells were pretreated with different doses of GF1 (10, 15, 20, 25, 30, 40, and 60 μM) for 30 minutes, before being challenged with THP (5 μM). Equal amounts of serum-free media were given to the cells in CON. Finally, cell viabilities were detected using the MTT assay.

2.10. Cell treatments

H9c2 cells were divided into five groups. Control group (CON): in which cells were cultured in serum-free DMEM high-glycemic culture medium; THP group (THP): cells were cultured in serum-free DMEM high-glycemic culture medium containing 5 μM THP; GF1 group (GF1): cells were treated with 40 μM GF1 30 min before addition of 5 μM THP; AKT inhibitor group (imidazoquinoxaline, IMQ) or Nrf2 inhibitor group (trigonelline): cells were treated with 1 μM IMQ or 150 μM trigonelline 30 min before treatment with 5 μM THP. In the GF1+ AKT inhibitor group (IMQ) or Nrf2 inhibitor group (trigonelline), serum-free DMEM high-glycemic culture medium containing 40 μM GF1 and 1 μM IMQ or 150 μM trigonelline were added 30 min before addition of 5 μM THP. Cells in the various groups were incubated for 24 h.

2.11. Western blotting analysis

Using sodium dodecyl sulfate-polyacrylamide gel electrophoresis (SDS-PAGE), equivalent amounts of protein samples were separated and transferred to a PVDF membrane [17]. The membranes were blocked with 5% milk in Tris-buffered saline (TBS), then incubated with the appropriate primary antibodies against AKT (1:1000), p-AKT (1:1000), pro-caspase 9 (1:1000), pro-caspase 3 (1:1000), cleaved-caspase 3 (1:1000), Bax (1:1000), Bcl-2 (1:1000), Nrf2 (1:500), Keap1 (1:1000), HO-1 (1:1000), Gst (1:1000), and GCLM (1:1000). The membranes were incubated at 4 °C overnight and rinsed three times before being incubated with secondary antibodies (1:5000) for 60 min, and enhanced chemiluminescence reagents were used to visualize the protein bands. A gel imaging system was used to examine the levels of protein expression (Alpha Imager2200, Alpha Innotech Corporation, San Leandro, CA, USA).

2.12. Statistical analysis

Differences in gray values of bands produced by Western blotting were analyzed using Image J software. The data were expressed using mean \pm SD, and all data were compared with SPSS 16.0 software, using one-way ANOVA and Duncan's Multiple Range Test. $P < 0.05$ denotes a statistically significant outcome.

3. Results

3.1. GF1 ameliorated rat body weight

As indicated in Table S1, rats in the THP group reveal significant weight loss compared with the CON group. Compared with THP group, the weight of rats in GF1L and GF1H groups significantly increased. In terms of relieving weight loss, GF1H group

outperformed Dexrazoxane (DZR) group, while GF1L group had no statistically significant difference from DZR group.

3.2. Effects of GF1 on THP-induced hemodynamics and electrocardiograph

Compared with CON group, THP group had significantly lower LVSP and $\pm\text{dp}/\text{dtmax}$ values, but the LVEDP value was significantly higher. Compared with the THP group, the DZR and GF1 groups have lower LVEDP values, whereas LVSP and $\pm\text{dp}/\text{dtmax}$ significantly increased. Compared with the DZR group, LVSP levels in rats in the GF1L group significantly increased; the LVEDP of rats in the GF1H group decreased, while LVSP and $\pm\text{dp}/\text{dtmax}$ significantly increased (Fig. 1A–D).

Compared with CON group, QRS complex voltage of THP group was significantly reduced, Q-T interval of rats was prolonged, and heart rate (HR) was significantly weakened. Compared with THP group, QRS complex voltage and HR of rats in DZR and GF1 groups increased significantly, but the Q-T interval was shortened. The GF1H group outperformed DZR group on various electrocardiogram indicators (Fig. 1E–G).

3.3. Effects of GF1 on THP-induced myocardial enzymes

Myocardial enzymes are commonly used indicators in myocardial injury (Fig. 1H–K). The serum LDH, CKMB, c-TnT, and BNP levels of rats in the THP group are significantly higher than in the CON group. Compared with the THP group, DZR and GF1 rats had significantly reduced LDH, CKMB, c-TnT, and BNP content. The GF1H group reveals a better reduction of LDH, c-TnT, and BNP content than DZR rats.

3.4. Effects of GF1 on THP-induced oxidative stress in rats heart tissue

Compared with the CON group, the THP group exhibits a decrease in rat serum SOD and GSH levels and an increase in MDA content. Compared with the THP group, DZR, GF1L, and GF1H groups had significantly increased SOD and GSH levels and reduced MDA content (Fig. 2A–C).

The expression levels of nuclear Nrf2, HO-1, Gst, and GCLM in THP group were significantly lower than in the CON group, while those of cytoplasmic Nrf2 and Keap1 were significantly higher. Nuclear Nrf2, HO-1, Gst, and GCLM expression levels in DZR, GF1L, and GF1H groups were significantly higher than in the THP group; however, cytoplasmic Nrf2 and Keap1 expression levels were significantly lower. Compared with the DZR group, the expression level of nuclear Nrf2 was higher in the GF1L group, and the expression level of nuclear Nrf2, HO-1, Gst, and GCLM increased significantly in the GF1H group (Fig. 2D–J).

3.5. Effect of GF1 on THP-induced myocardial histopathological change

The pathological changes in myocardial tissue are illustrated in Fig. 2K and L. HE staining reveals that the myocardial tissue of the CON group is normal, with no visible hypertrophy of myocardial cells or inflammatory cell infiltration. After THP treatment, rat myocardial fibers are arranged irregularly, myocardial cells are edematous, gaps are significantly widened, and cytoplasmic lysis can produce vacuolar degeneration and inflammatory cell infiltration. All these changes indicate severe myocardial damage. After GF1 and DZR intervention, the intercellular space is reduced, the arrangement becomes more regular, and vacuole-like degeneration

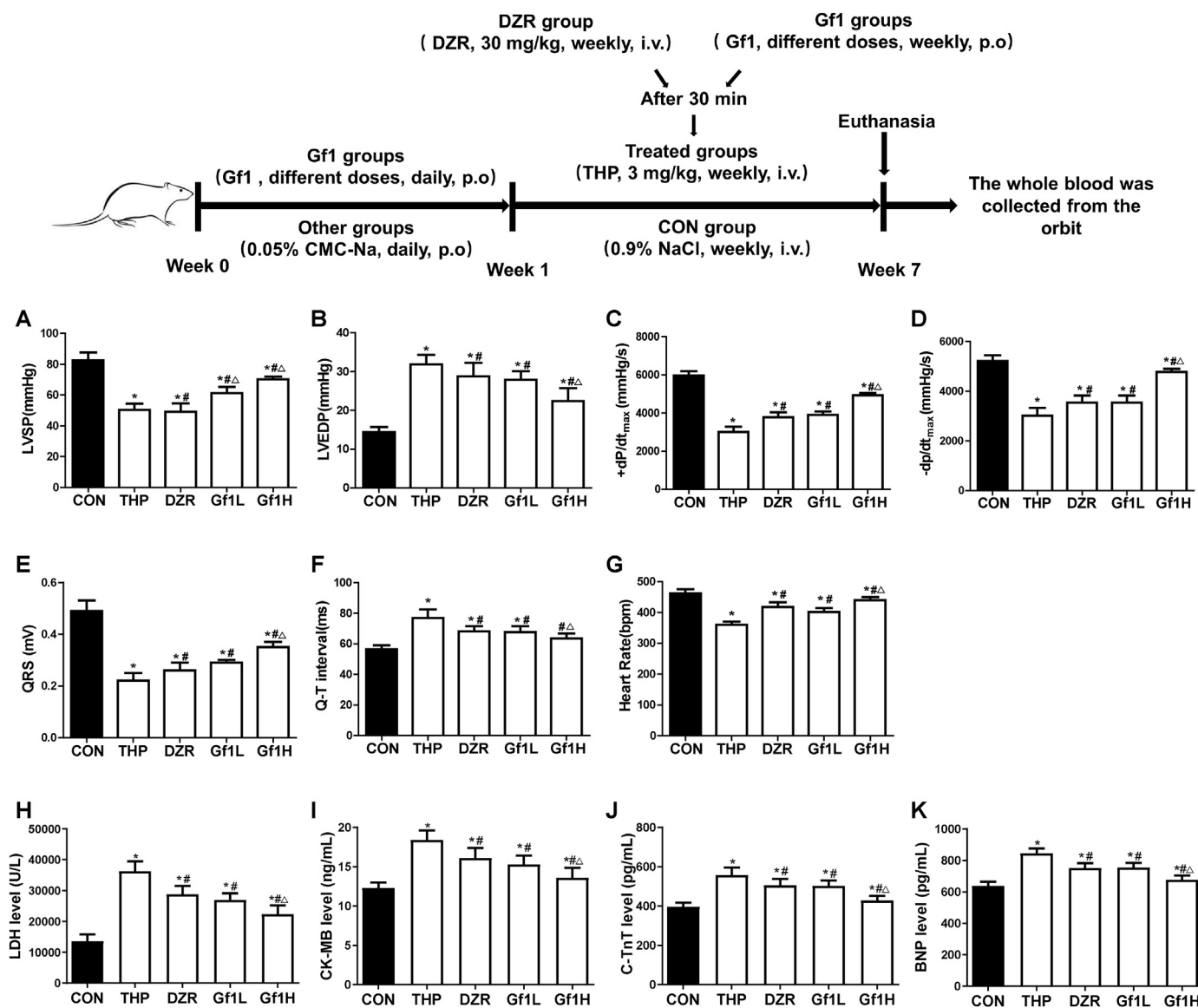


Fig. 1. GF1's effects on THP-induced hemodynamic indices, electrocardiograms, and serum cardiac enzymes in rats. (A) Left ventricular systolic pressure (LVSP); (B) left ventricular end-diastolic pressure (LVEDP); (C and D) maximal left ventricular pressure change ($\pm dp/dt_{max}$); (E) cardiac QRS complex; (F) representative cardiac Q-T interval; (G) representative heart rate; (H) representative levels of lactate dehydrogenase (LDH); (I) representative levels of creatine kinase MB (CK-MB); (J) representative cardiac troponin T levels (c-TnT); and (K) representative brain natriuretic peptide levels (BNP). *P < 0.05 in comparison to the CON group; #P < 0.05 in comparison to the THP group; Δ P < 0.05 in comparison to the DZR group. Each data value represents mean \pm SD of in each group (n = 6).

is reduced in a scattered distribution. The GF1H group has the most significant improvement in reducing vacuole degeneration.

3.6. GF1 attenuates the expression of apoptosis-related proteins

The CON group has very low levels of cyt-c and p-AKT expression. After THP exposure, the positive expression of cyt-c is obvious, but p-AKT expression is further reduced. Compared with THP group, the positive expression of cyt-c was significantly reduced in GF1L and GF1H groups, and p-AKT expression was significantly increased. The GF1H group has a better effect on lowering cyt-c protein level and increasing p-AKT protein level than the DZR group (Fig. 3A–D).

The level of caspase 3 protein in the CON group is low. After THP exposure, the expression of caspase 3 protein is evident. Compared with the THP group, the expression levels of caspase 3 in the GF1L

and GF1H groups are significantly reduced. The effect of reducing the expression level of caspase 3 in the GF1H group outperforms that in the DZR group (Fig. 3E and F).

3.7. Effect of GF1 on AKT/ Bcl-2 signaling pathway in rats heart tissue

Compared with the CON group, the expression levels of p-AKT/ AKT, pro-caspase 9, pro-caspase 3, and Bcl-2/Bax ratio in the THP group are considerably lower, but the level of cleaved-caspase 3 is significantly higher. In the DZR, GF1L, and GF1H groups, the expression levels of p-AKT/ AKT, pro-caspase 9, pro-caspase 3, and Bcl-2/Bax ratio are considerably higher than in the THP group, whereas the level of cleaved-caspase 3 is significantly lower. The expression levels of pro-caspase 3 and cleaved-caspase 3 in the GF1L group are considerably higher than in the DZR group; the

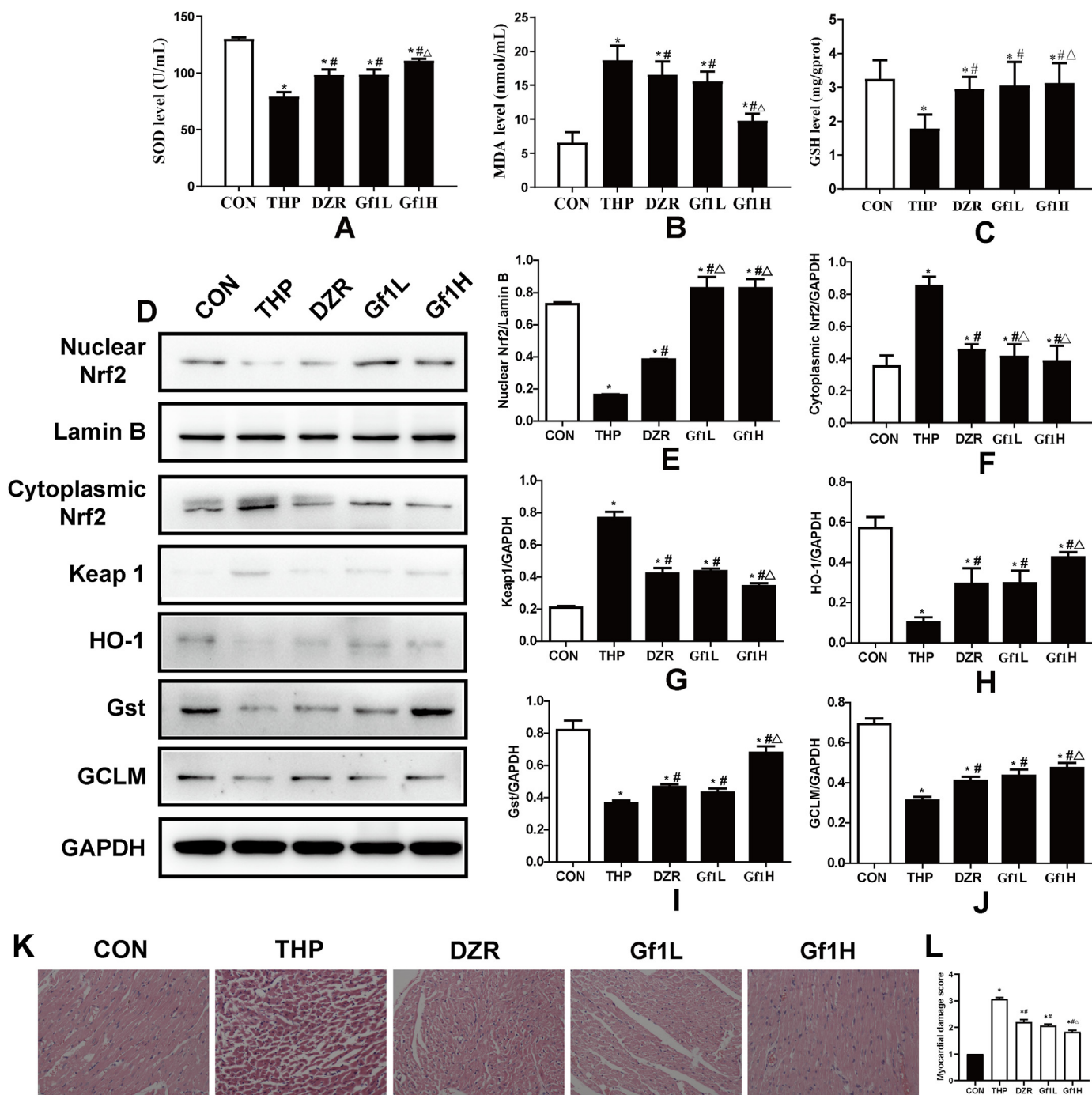


Fig. 2. Effects of GF1 on rat cardiac oxidative stress and histological alterations produced by THP. (A) Superoxide dismutase (SOD) levels; (B) malondialdehyde (MDA) content; (C) glutathione (GSH) levels; (D) representative Nrf2 levels in the nucleus; in the nucleus Lamin B was employed as an internal control. Protein expression of Nrf2, keap1, HO-1, Gst, and GCLM in the cytoplasm; GAPDH was employed as an internal control in the cytoplasm; (E) protein ratios of Nrf2 and Lamin B in the nucleus; (F) protein ratios of Nrf2 and GAPDH in the cytoplasm; (G–J) protein ratios of cytosolic keap1, HO-1, Gst, and GCLM and GAPDH. *P < 0.05 in comparison to the CON group; #P < 0.05 in comparison to the THP group; △P < 0.05 in comparison to the DZR group. Each data value represents mean ± SD of in each group (n = 3). (K) Staining using H&E (200× magnification; n = 6); (L) HE staining is scored on a five-point scale from 0 to 4.

expression levels of p-AKT/AKT and pro-caspase 3 in the GF1H group are significantly higher than those in the DZR group (Fig. 3G–L).

3.8. GF1 reduces THP-induced H9c2 cells damage

At time points 6, 12, 24, and 36 h, cell viability in each group did not change significantly, indicating that GF1 has no toxic effect on

H9c2 cells (Fig. 4A). The screening was continued to determine the optimal concentration and time for THP-induced damage to H9c2 cells. Compared with the CON group, cell survival rates at different time points were higher than 70% after treatment with 1 and 3 μM THP; treatment with 7 and 9 μM THP for 6 h and after 12 h revealed a cell survival rate higher than 70%. After 24 h and 36 h, the cell survival rate was lower than 50%, and the cell survival rate was too low; only the survival rate of H9c2 cells treated with 5 μM THP for

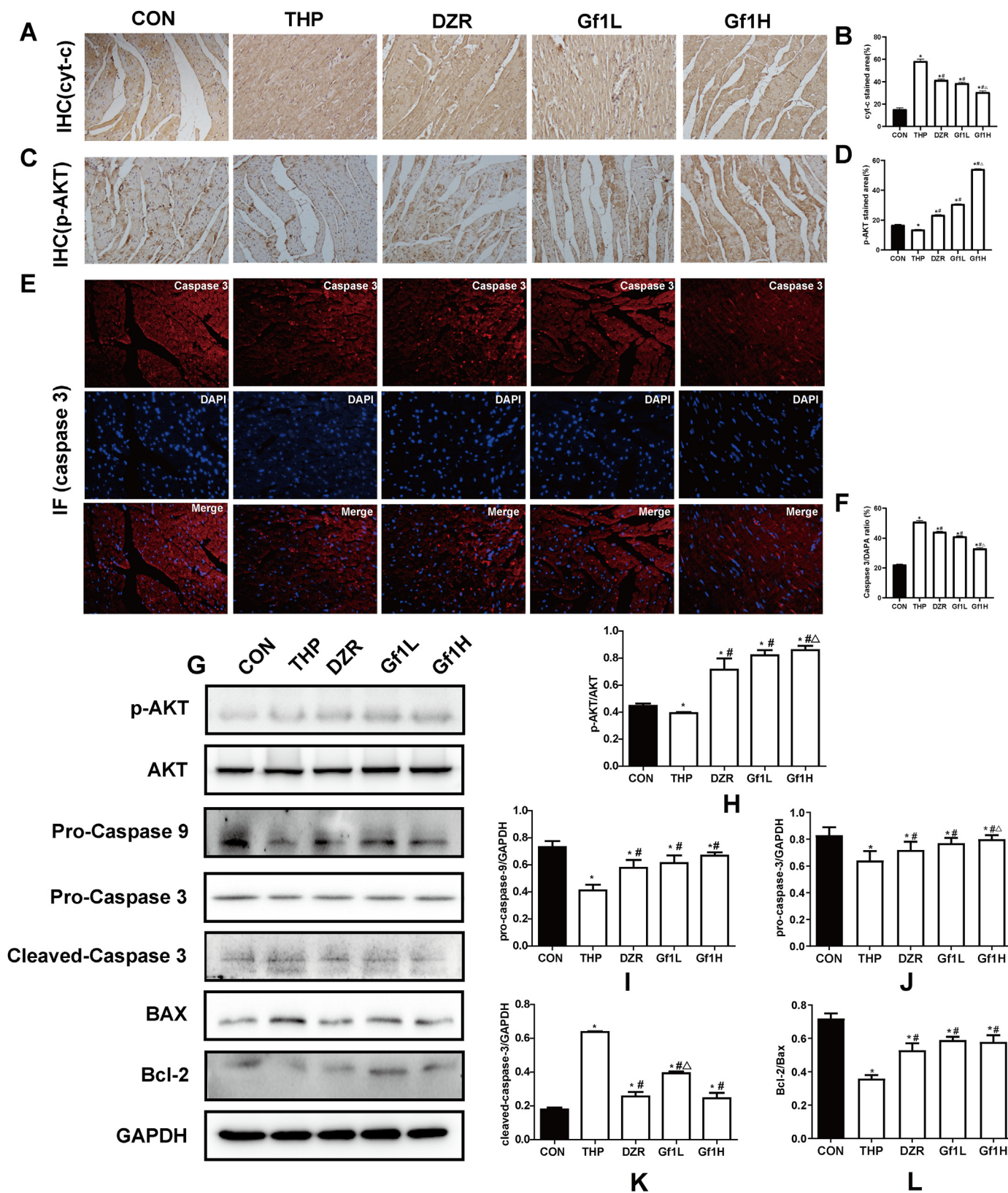


Fig. 3. THP-induced related-protein expression in rat cardiac tissue and the effects of GF1. (A) Immunohistochemistry pictures of cyt-c in cardiac tissue from rats; (B) Image-Pro Plus 6.0 software was used to assess the immunohistochemistry intensity of cyt-c expression; (C) Immunohistochemistry pictures of p-AKT in cardiac tissue from rats; (D) Image-Pro Plus 6.0 software was used to assess the immunohistochemical intensity of p-AKT expression; (E) Representative caspase 3 immunofluorescence images in rat cardiac tissue; (F) Image-Pro Plus 6.0 software was used to evaluate the fluorescence intensity of caspase 3; (G) Protein expression of the p-AKT, Bcl-2, Bax, and caspase families; GAPDH was used as an internal control; (H) p-AKT and AKT protein ratios; (I–K) representative caspase family and GAPDH ratios; (L) Bcl-2 and Bax ratios. *P < 0.05 in comparison to the CON group; #P < 0.05 in comparison to the THP group; Δ P < 0.05 in comparison to the DZR group. Each data value represents mean \pm SD of in each group (n = 3).

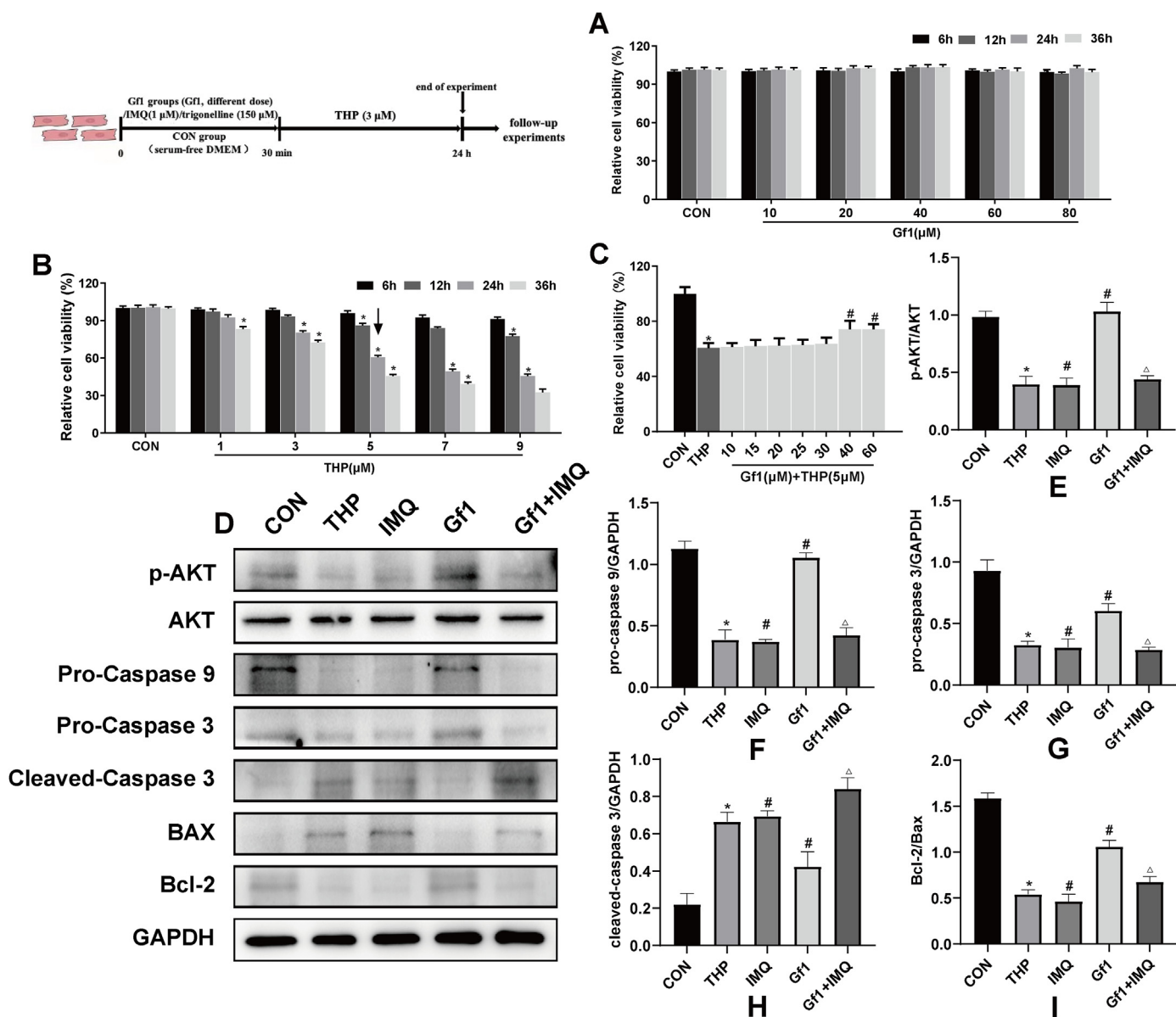


Fig. 4. H9c2 cells were protected from THP-induced apoptosis by GF1. (A) GF1 cytotoxicity on H9c2 cells. **p* < 0.05 vs. 0 μM group (*n* = 6); (B) THP effect on H9c2 cell survival rate. **p* < 0.05 compared to the CON group (*n* = 6); (C) representative of GF1 effects on H9c2 cell viability induced by THP (*n* = 6); (D) representative p-AKT, Bcl-2, Bax, and caspase family protein expression; GAPDH was used as an internal control; (E) representative p-AKT and AKT protein ratios; (F–H) representative caspase family and GAPDH protein ratios; (I) representative Bcl-2 and Bax ratios. **P* < 0.05 in comparison to CON group; #*P* < 0.05 in comparison to THP group; △*P* < 0.05 in comparison to GF1 group. Each data value represents mean ± SD of in each group (*n* = 3).

24 h was higher than 60%, while that of H9c2 cells treated with 5 μM THP for 36 h was less than 50%, and the cell survival rate was too low. Therefore, the optimal concentration and time of THP-induced H9c2 cell injury model were selected as 5 μM and 24 h, respectively (Fig. 4B).

Furthermore, the viability of H9c2 cells treated with 5 μM THP was once drastically reduced compared to the CON group. However, GF1 at the doses of 40 and 60 μM considerably elevated the viabilities of H9c2 cells compared to the THP group (Fig. 4C). Therefore, an GF1 concentration of 40 μM was determined to reduce the damage in THP-induced H9c2 cells.

3.9. GF1 reduces THP-induced apoptosis through AKT/Bcl-2 signaling pathway in H9c2 cells

The expression levels of p-AKT/AKT, pro-caspase 9, pro-caspase 3, and Bcl-2/Bax ratio in the THP group are considerably lower than in the CON group, but the level of cleaved-caspase 3 is significantly higher. The expression levels of p-AKT/AKT, pro-caspase 9, pro-caspase 3, and the Bcl-2/Bax ratio in the IMQ group are considerably lower than in the THP group, while the level of cleaved-caspase 3 is significantly higher, whereas the GF1 group had the opposite outcome. The expression levels of p-AKT/AKT, pro-caspase 9, pro-caspase 3, and the Bcl-2/Bax ratio in the GF1+IMQ group are considerably lower than in the GF1 group, but the level of cleaved-caspase 3 is significantly higher (Fig. 4 D–I).

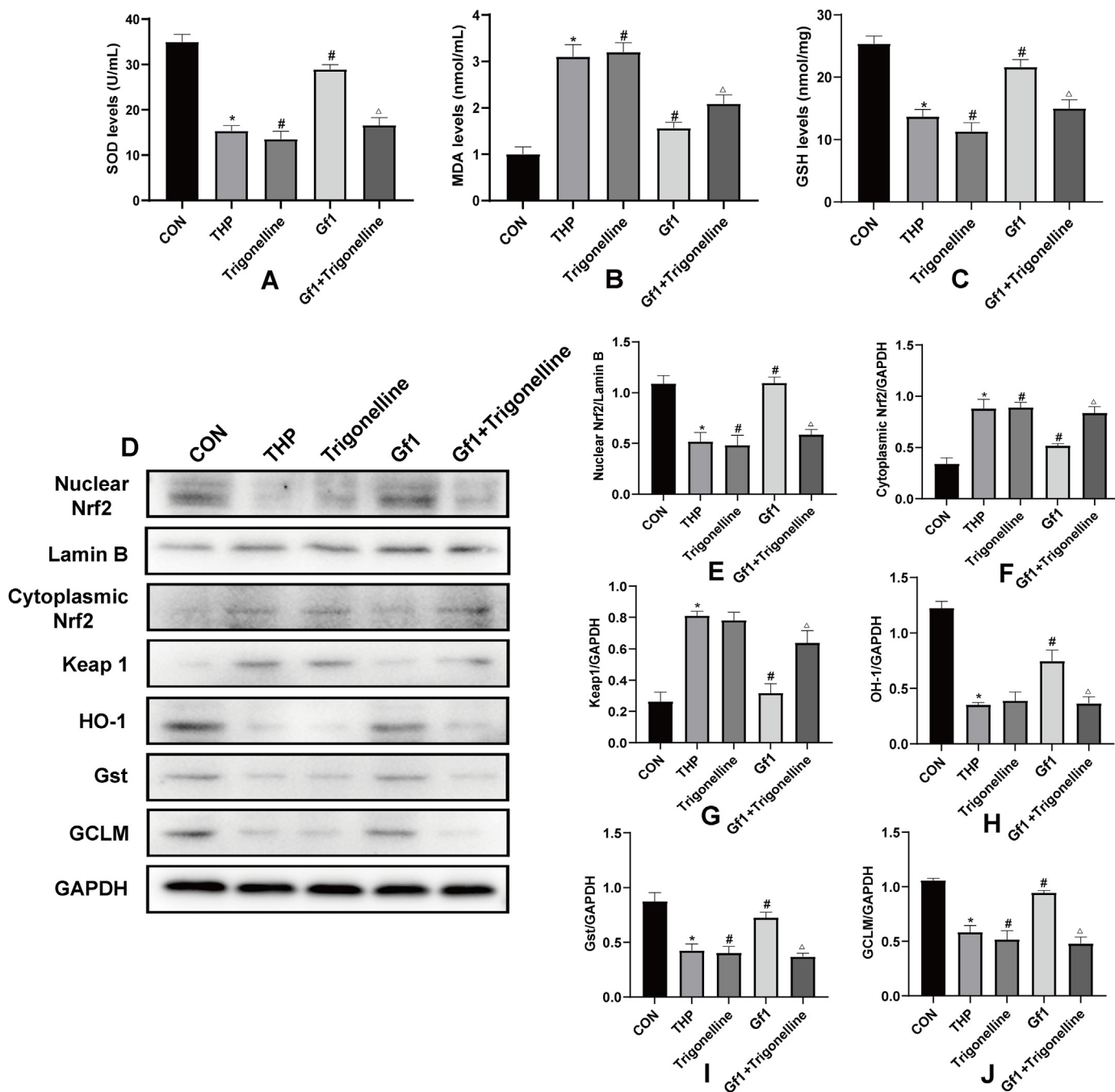


Fig. 5. THP-induced oxidative stress in H9c2 cells and the effects of GF1. (A) Representative levels of superoxide dismutase (SOD); (B) representative levels of malondialdehyde (MDA); (C) representative levels of glutathione (GSH); (D) representative Nrf2 levels in nucleus; Lamin B was used as an internal control in nucleus; Nrf2, keap1, HO-1, Gst, and GCLM protein expression in cytoplasm; GAPDH was utilized as an internal control in cytoplasm; (E) representative nucleus Nrf2 and Lamin B protein ratio; (F) representative cytosolic Nrf2 and GAPDH protein ratios; and (G-J) representative cytosolic keap1, HO-1, Gst, and GCLM and GAPDH protein ratios. *P < 0.05 in comparison to CON group; #P < 0.05 in comparison to THP group; Δ P < 0.05 in comparison to GF1 group. Each data value represents mean \pm SD of in each group (n = 3).

3.10. GF1 reduces THP-induced oxidative stress in H9c2 cells

Compared with the CON group, the THP group significantly increased MDA content while decreasing SOD and GSH levels in H9c2 cells. Compared with the THP group, the trigonelline group markedly increased MDA content and reduced SOD and GSH levels; GF1 significantly decreased MDA content and increased SOD and GSH levels. Compared with the GF1 group, the GF1 + trigonelline

group decreased SOD and GSH levels while increasing MDA content (Fig. 5A–C).

The expression levels of nuclear Nrf2, HO-1, Gst, and GCLM in the THP group are significantly lower than in the CON group, while those of cytoplasmic Nrf2 and Keap1 are significantly higher. The expression levels of nuclear Nrf2, Gst, and GCLM in the trigonelline group are significantly lower than in the THP group, while that of cytoplasmic Nrf2 is significantly higher, although the levels of HO-1 and Keap1 are unchanged. Nuclear Nrf2, HO-1, Gst, and GCLM

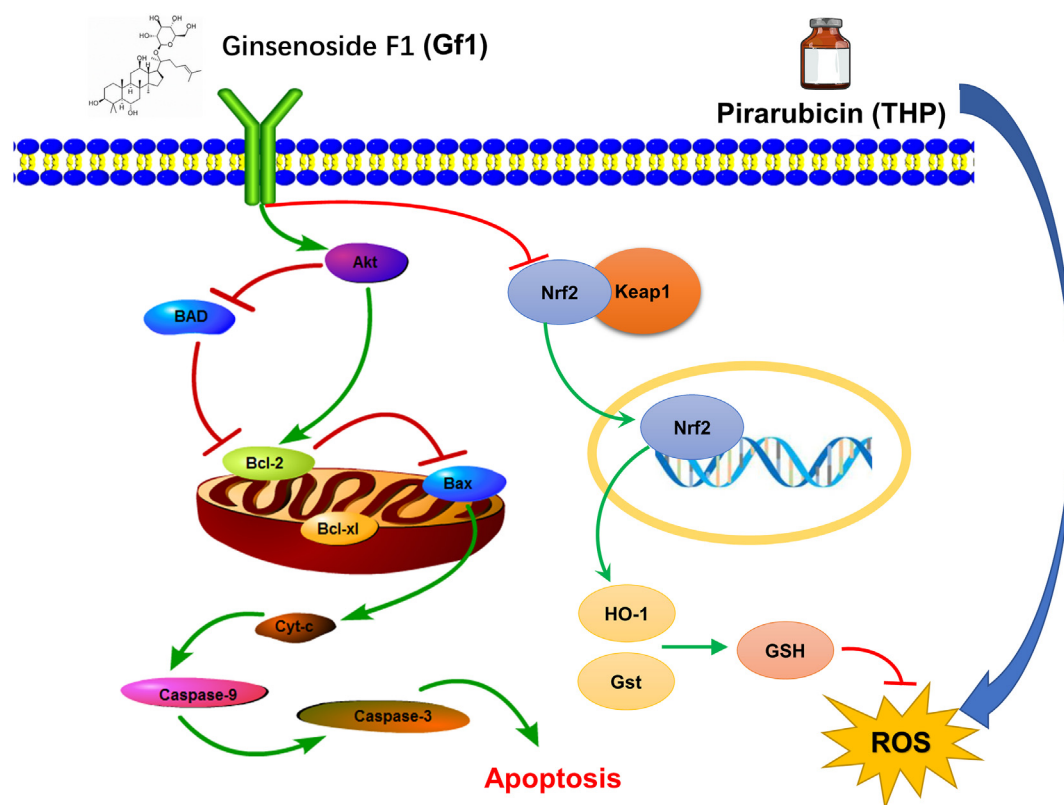


Fig. 6. Scheme summarizes GF1 against THP-induced myocardial toxicity via activation Nrf2 and AKT/Bcl-2 signaling pathways to inhibit oxidative stress and apoptosis.

expression levels in the GF1 group are considerably higher than in the THP group, but cytoplasmic Nrf2 and Keap1 expression levels are significantly lower. Nuclear Nrf2, HO-1, Gst, and GCLM expression levels are lower in the GF1 + trigonelline group compared to the GF1 group, but cytoplasmic Nrf2 and Keap1 expression levels are higher (Fig. 5D–J).

4. Discussion

Cardiotoxicity is the most serious toxicity of THP and is often progressive and irreversible, eventually resulting in heart failure and death [3,19]. As a result, it is particularly important to actively prevent and monitor THP-induced cardiotoxicity.

We measured body weight, hemodynamic indicators, electrocardiogram, and the content of related myocardial enzymes. Our group has adopted a regimen of a single tail vein injection of 3 mg/kg THP once a week for six weeks, accurately replicating a rat model of THP-induced myocardial injury. THP entered the body of rats, causing weight loss and impaired cardiac function. Shi et al. found that after intravenous injection of 3 mg/kg THP for eight weeks, a series of systemic and cardiac toxicity changes occurred in SD rats, including abnormal body weight and food intake, adverse changes in echocardiography and electrocardiogram readings, and cardiac tissue structure damage [20]. Following GF1 treatment, the rats' cardiac function was partially restored, and their weight increased. The results indicate that GF1 treatment can significantly reduce the changes in THP-induced cardiac function. Zhang et al. found that GF1 administration increases cerebral micro vessel density and improves focal blood perfusion in ischemic regions of rats subjected to MCAO [21]. The above experiments show that GF1 has a therapeutic effect on cardiovascular and cerebrovascular diseases.

Additionally, HE results reveal that GF1 can significantly attenuate THP-induced structural changes in cardiomyocytes. Cardiac markers, such as c-TnT, LDH, CK-MB, and BNP, have been employed clinically to diagnose myocardial necrosis. Zhang et al. showed that DOX caused a significant increase in intracellular space, cytoplasmic vacuolation, and myocardial cell disorders, with plasma BNP, CK-MB, CTnT, and LDH activities significantly elevated [16]. His findings are consistent with the experimental findings of this study, whereby GF1 administration decreased serum marker levels and reversed these changes in cardiac morphology. At the same time, it has been found that GF1 also has anti-atherosclerosis pharmacological effects. Qin et al. found that GF1-treated mice had a significantly reduced lesion size compared with model group mice [22].

Currently, the mechanism of anthracycline-induced cardiotoxicity is mainly based on the oxidative stress theory and its dependent molecular pathways [23]. The heart tissue has a shallow content of antioxidant enzymes, has a limited ability to resist oxidation, and is more sensitive to ROS [24]. Elevated serum MDA, diminished serum SOD, and GSH levels have been determined in this study, indicating that THP can cause oxidative stress. Wang et al. also showed that treatment with pirarubicin alone significantly decreased serum SOD levels compared to the normal control group [4]. In our investigation, GF1 at a dose of 25–50 mg/kg, or 40 M, significantly reduced serum MDA and increased serum SOD and GSH levels, demonstrating that GF1 has antioxidant characteristics. Furthermore, GF1 has been shown to have notable antioxidant effects in various cardiac tissue disease models. Wang et al. suggested that GF1 attenuated oxidative stress-induced mitochondrial damage in cardiomyocytes by activating SIRT1 [25].

By regulating oxidative stress, Nrf2 is thought to act as an endogenous suppressor of THP-induced cardiac toxicity [26]. Zhao et al. showed DOX-induced cardiotoxicity by promoting myocardial

oxidative stress via targeting Nrf2 and Sirt2 [27]. By activating the Keap1/Nrf2/ARE antioxidant pathway, GF1 substantially reduces triptolide-induced cytotoxicity in HL-7702 cells [28]. In this investigation, we discovered that THP decreased Nrf2 expression in the nucleus in both *in vitro* and *in vivo* experiments. Furthermore, we discovered that GF1 increased Nrf2 nuclear translocation, influencing the expression levels of HO-1, Gst, GCLM, and Keap1, as well as reducing THP-induced cardiac oxidative stress. The aforesaid GF1 actions are diminished when trigonelline (an Nrf2 inhibitor) is added.

Bcl-2, an anti-apoptotic protein and a regulator of apoptotic genes, primarily regulates apoptosis via mitochondria [29]. When the outer mitochondrial membrane permeability changes, cyto-c is released into the cytoplasm, apoptosis-inducing factors are released, and the caspase cascade response is initiated [30]. AKT is at the center of multiple pathways. AKT can mediate apoptosis and phosphorylate Bax, a member of the Bcl-2 family to regulate apoptosis [31]. Wang *et al.* observed that compared with the control group, the THP group had significantly lower p-PI3K, p-Akt, and p-mTOR [32]. In our study, in comparison to the CON group, THP treatment increased cytoplasmic cyto-c levels and cleaved-caspase 3 protein expression while lowering Bcl-2/Bax and p-AKT/AKT ratios. Compared to the THP-only group, GF1 treatment dramatically increased Bcl-2/Bax and p-AKT/AKT ratios, as well as pro-caspase 9 and pro-caspase 3, while lowering cyto-c in the cytoplasm and cleaved-caspase 3 levels. The aforesaid GF1 actions are diminished when imidazoquinoline (an AKT inhibitor) is added. Lee *et al.* investigated that protection from ultraviolet-B-induced apoptosis is tightly correlated with GF1 mediated inhibition of ultraviolet-B-induced downregulation of Bcl-2 and Brn-3a expression [33]. These experiments indicate that the anti-apoptotic effect of GF1 is related to the AKT/Bcl-2 signaling pathway.

Finally, our findings showed that GF1 significantly reduced THP-induced cardiotoxicity by modifying Nrf2 and AKT/Bcl-2 signaling pathways, reducing myocardial oxidative stress and apoptosis (Fig. 6). Indeed, more research into the underlying processes and clinical applications of this natural substance against THP-induced cardiotoxicity is needed.

Author contributions

Yang Zhang, Jiu-Long Ma and Li-Qun Ren conceived and designed the experiments. Yang Zhang and Jiu-Long Ma performed the experiments. Shan Liu, Chen Chen, Qi Li, and Meng Qin contributed to the preparation of reagents and analyzed the data. All data were generated in-house, and no paper mill was used. All authors agree to be accountable for all aspects of work ensuring integrity and accuracy.

Declaration of competing interest

The authors declare no conflicts of interest in this work.

Acknowledgements

This work was supported by funding from the National Natural Science Foundation of China (No. 81773934).

Appendix A. Supplementary data

Supplementary data to this article can be found online at <https://doi.org/10.1016/j.jgr.2022.06.002>.

References

- [1] Rivankar S. An overview of doxorubicin formulations in cancer therapy. *J Cancer Res Ther* 2014;10:853–8.
- [2] Zhao H, Yao Y, Wang Z, Lin F, Sun Y, Chen P. Therapeutic effect of pirarubicin-based chemotherapy for osteosarcoma patients with lung metastasis. *J Chemother* 2010;22:119–24.
- [3] Valcovici M, Andrica F, Serban C, Dragan S. Cardiotoxicity of anthracycline therapy: current perspectives. *Arch Med Sci* 2016;12:428–35.
- [4] Wang YD, Zhang Y, Sun B, Leng XW, Li YJ, Ren LQ. Cardioprotective effects of rutin in rats exposed to pirarubicin toxicity. *J Asian Nat Prod Res* 2018;20:361–73.
- [5] Kim JK, Cui CH, Yoon MH, Kim SC, Im WT. Bioconversion of major ginsenosides Rg1 to minor ginsenoside F1 using novel recombinant ginsenoside hydrolyzing glycosidase cloned from *Sanguibacter keddiei* and enzyme characterization. *J Biotechnol* 2012;161:294–301.
- [6] Kim JH, Baek EJ, Lee EJ, Yeom MH, Park JS, Lee KW, Kang NJ. Ginsenoside F1 attenuates hyperpigmentation in B16F10 melanoma cells by inducing dendrite retraction and activating Rho signalling. *Exp Dermatol* 2015;24:150–2.
- [7] Wang Y, Choi KD, Yu H, Jin F, Im WT. Production of ginsenoside F1 using commercial enzyme Cellulase KN. *J Ginseng Res* 2016;40:121–6.
- [8] Wang F, Pu C, Zhou P, Wang P, Liang D, Wang Q, Hu Y, Li B, Hao X. Cinnamaldehyde prevents endothelial dysfunction induced by high glucose by activating Nrf2. *Cell Physiol Biochem* 2015;36:315–24.
- [9] Luo C, Urgard E, Voorder T, Metspalu A. The role of COX-2 and Nrf2/ARE in anti-inflammation and antioxidative stress: aging and anti-aging. *Med Hypotheses* 2011;77:174–8.
- [10] Tran PL, Kim O, Tran HNK, Tran MH, Min BS, Hwangbo C, Lee JH. Protective effects of extract of *Cleistocalyx operculatus* flower buds and its isolated major constituent against LPS-induced endotoxemic shock by activating the Nrf2/HO-1 pathway. *Food Chem Toxicol* 2019;129:125–37.
- [11] Chen QM. Nrf2 for cardiac protection: pharmacological options against oxidative stress. *Trends Pharmacol Sci* 2021;42:729–44.
- [12] Zhang Y, Ma XY, Zhang T, Qin M, Sun B, Li Q, Hu DW, Ren LQ. Protective effects of apocynin against pirarubicin-induced cardiotoxicity. *Am J Chin Med* 2019;47:1075–97.
- [13] Das S, Steenbergen C. Mitochondrial adenine nucleotide transport and cardioprotection. *J Mol Cell Cardiol* 2012;52:448–53.
- [14] Alvarez S, Valdez LB, Zaobornyj T, Boveris A. Oxygen dependence of mitochondrial nitric oxide synthase activity. *Biochem Biophys Res Commun* 2003;305:771–5.
- [15] Adam-Vizi V, Chinopoulos C. Bioenergetics and the formation of mitochondrial reactive oxygen species. *Trends Pharmacol Sci* 2006;27:639–45.
- [16] Zhang Y, Ma C, Liu C, Wei F. Luteolin attenuates doxorubicin-induced cardiotoxicity by modulating the PHLPP1/AKT/Bcl-2 signalling pathway. *PeerJ* 2020;8:e8845.
- [17] Wang CM, Li HF, Wang XK, Li WG, Su Q, Xiao X, Hao TF, Chen W, Zhang YW, Zhang HY, et al. Ailanthus Altissima-derived Ailanthone enhances Gastric Cancer Cell Apoptosis by Inducing the Repression of Base Excision Repair by Downregulating p23 Expression. *Int J Biol Sci*. 2021;17:2811–25.
- [18] Zhu W, Ding J, Sun L, Wu J, Xu X, Wang W, Li H, Shen H, Li X, Yu Z, et al. Heterogeneous nuclear ribonucleoprotein A1 exerts protective role in intracerebral hemorrhage-induced secondary brain injury in rats. *Brain Res Bull* 2020;165:169–77.
- [19] Zhang J, Cui X, Yan Y, Li M, Yang Y, Wang J, Zhang J. Research progress of cardioprotective agents for prevention of anthracycline cardiotoxicity. *Am J Transl Res* 2016;8:2862–75.
- [20] Shi H, Tang H, Ai W, Zeng Q, Yang H, Zhu F, Wei Y, Feng R, Wen L, Pu P, et al. Schisandrin B antagonizes cardiotoxicity induced by pirarubicin by inhibiting mitochondrial permeability transition pore (mPTP) opening and decreasing cardiomyocyte apoptosis. *Front Pharmacol* 2021;12:733805.
- [21] Zhang J, Liu M, Huang M, Chen M, Zhang D, Luo L, Ye G, Deng L, Peng Y, Wu X, et al. Ginsenoside F1 promotes angiogenesis by activating the IGF-1/IGF1R pathway. *Pharmacol Res* 2019;144:292–305.
- [22] Qin M, Luo Y, Lu S, Sun J, Yang K, Sun J, Yang K, Sun G, Sun X. Ginsenoside F1 ameliorates endothelial cell inflammatory injury and prevents atherosclerosis in mice through A20-mediated suppression of NF-κB signaling. *Front Pharmacol* 2017;8:953.
- [23] Songbo M, Lang H, Xinyong C, Bin X, Ping Z, Liang S. Oxidative stress injury in doxorubicin-induced cardiotoxicity. *Toxicol Lett* 2019;307:41–8.
- [24] Sun XP, Wan LL, Yang QJ, Huo Y, Han YL, Guo C. Scutellarin protects against doxorubicin-induced acute cardiotoxicity and regulates its accumulation in the heart. *Arch Pharm Res* 2017;40:875–83.
- [25] Wang Y, Liang X, Chen Y, Zhao X. Screening SIRT1 activators from medicinal plants as bioactive compounds against oxidative damage in mitochondrial function. *Oxid Med Cell Longev* 2016;2016:4206392.
- [26] Jing L, Yang M, Li Y, Yu Y, Liang B, Cao L, Zhou X, Peng S, Sun Z. Metallothionein prevents doxorubicin cardiac toxicity by indirectly regulating the uncoupling proteins 2. *Food Chem Toxicol* 2017;110:204–13.
- [27] Zhao L, Qi Y, Xu L, Tao X, Han X, Yin L, Peng J. MicroRNA-140-5p aggravates doxorubicin-induced cardiotoxicity by promoting myocardial oxidative stress via targeting Nrf2 and Sirt2. *Redox Biol* 2018;15:284–96.

- [28] Peng H, You L, Yang C, Wang K, Liu M, Yin D, Xu Y, Dong X, Yin X, Ni J. Ginsenoside Rb1 attenuates triptolide-induced cytotoxicity in HL-7702 cells via the activation of keap1/Nrf2/ARE pathway. *Front Pharmacol* 2021;12:723784.
- [29] Lindsay J, Esposti MD, Gilmore AP. Bcl-2 proteins and mitochondria-specificity in membrane targeting for death. *Biochim Biophys Acta* 2011;1813:532–9.
- [30] Song XF, Tian H, Zhang P, Zhang ZX. Expression of cyt-c-mediated mitochondrial apoptosis-related proteins in rat renal proximal tubules during development. *Nephron* 2017;135:77–86.
- [31] Manning BD, Toker A. AKT/PKB signaling: Navigating the Network. *Cell* 2017;169:381–405.
- [32] Wang F, Wang L, Jiao Y, Wang Z. Qishen Huanwu capsule reduces pirarubicin-induced cardiotoxicity in rats by activating the PI3K/Akt/mTOR pathway. *Ann Palliat Med* 2020;9:3453–61.
- [33] Lee EH, Cho SY, Kim SJ, Shin ES, Chang HK, Kim DH, Yeom MH, Woe KS, Lee J, Sim YC, et al. Ginsenoside F1 protects human HaCaT keratinocytes from ultraviolet-B-induced apoptosis by maintaining constant levels of Bcl-2. *J Invest Dermatol* 2003;121:607–13.